A Smart Hollow Filament with Thermal Sensitive Internal Diameter

Qinghao Meng, Jinlian Liu, Liming Shen, Yang Hu, Jianping Han

Institute of Textiles and Clothing, The Hong Kong Polytechnic University, Hong Kong, People's Republic of China

Received 27 December 2007; accepted 29 November 2008
DOI 10.1002/app.30203
Published online 28 April 2009 in Wiley InterScience (www.interscience.wiley.com).

ABSTRACT: In this work, a thermoplastic shape memory polyurethane was prepared via melt polymerization and a corresponding shape memory hollow fiber was fabricated via melt spinning. The fiber mechanical properties, especially shape memory effect, were characterized by static tensile, thermo-mechanical cyclic tensile testing. The hollow fiber switching temperature was the melting transition temperature of the soft segment phase at about 41°C. The tenacity of the hollow fiber was about 1.14 cN/dtex, and breaking elongation was 682%. The shape fixity ratio was above 87% and the recovery ratio was above 89%. The internal diameter of the hollow fiber could be noticeably changed and the deformed fiber cross-section could be well fixed. Once heated above the soft segment phase melting transition temperature, the hollow fiber internal hole recovered to its original diameter. The results from differential scanning calorimetry, X-ray diffraction, and dynamic mechanical analysis were used to illustrate the mechanism governing the mechanical properties and shape memory effect especially. Due to the changes of the hollow fiber and the internal diameter affect of the physical properties of the prepared products, this fiber may be used in smart textiles for thermal management, or as stuffing of pillows and mattresses, which can adjust to body contours. Furthermore, the findings suggest that this kind of hollow fiber with thermal sensitive internal diameter could be used in smart filtration, drug-controlled release, and liquid transportation *in vivo*. © 2009 Wiley Periodicals, Inc. J Appl Polym Sci 113: 2440–2449, 2009

Key words: fibers; phase; separation; polyurethane

INTRODUCTION

The smart polyurethane is a class of polyurethanes that is different from conventional polyurethanes in that it not only has a segmented structure but a prominent glass transition (T_g type) or melting transition (T_m type) at around or slightly above an ambient temperature. Smart polyurethane may be synthesized from three starting materials: long-chain polyol, diisocyanate, and chain extender. Diisocyanate and chain extender form the hard segment and the long chain polyol forms the soft segment. Also, it may be synthesized with two kinds of long-chain polyols coupled with diisocyanate where one polyol with a higher thermal transition acts as a hard segment and another polyol acts as a soft segment.[1–4]

Smart polyurethanes are not very difficult to synthesize. In addition, some kinds of smart polyurethanes can be processed by using conventional techniques (injection, extrusion, blowing) to desire formats. They have found broad applications in textiles, automotive parts, building and construction products, intelligent packing, implantable medical devices, sensors, and actuators in the form of solution, emulsion, film, fiber, foam, and bulk.[5–7]

Presently the most extensively and intensively studied smart properties of smart polyurethanes are tunable mass transfer and shape memory properties.[6,8–13] Due to their special properties, smart polyurethanes have been used for thermal insulating fabrics, breathable fabrics, shoes, and crease- and shrink-resistant apparel fabrics.[8,14–17] Processes for making such products include finishing, coating, laminating, blending, and other innovative structures.

A commercialized smart polyurethane membrane Diapex was developed by Miysubishi Heavy Industries. The permeability of the membrane changes in response to the weather and wearer's body temperature. The United States Army Soldier Systems Center [18] developed a wet/dry suit with a shape memory polymer membrane and insulation materials that kept the wearer warm in marine environments but did not inhibit perspiration on land. Hu and coworkers[19,20] developed water-borne shape memory polyurethane solution and emulsion to finish fabric. When the body temperature was low, the finished fabric remained less permeable and retained body heat. When the body was hot and perspired, it allowed the water vapor to escape into the

Correspondence to: J. Liu (tchujl@inet.polyu.edu.hk).
Contract grant sponsor: Hong Kong Innovation Technology Funding; contract grant number: GHS/088/04.

environment. In addition, because of the polyurethane shape memory effect, when the treated fabric was washed or worn at body temperature, the treated fabric achieved crease retentions, flat appearance, and wrinkle recovery effects.[21–24]

Recently, Meng and coworkers[9,10,25–27] developed shape memory polyurethane fiber via wet spinning and melt spinning methods. In comparison with its bulk counterpart, shape memory fibers possess outstanding mechanical properties and shape recovery force owning to their molecular orientation.

Also, shape memory polyurethane foams have been developed by Tobushi et al.[6,28] Because the foam is light and has a large variation in volume, high energy absorption property, and heat insulating property, the most promising application may be in the aerospace field. Lendlein and Marco[29,30] proposed using shape memory foam to help overweight patients lose weight. The implanted foam will inflate at the body temperature in the stomach, so it provides the patients with a feeling of satiety. More interestingly, shape-memory foams have been proposed as measuring tools to survey the shape of complex cavities such as a human ear canal, so a hearing aid shape can be precisely made.[31]

One of the most attractive applications of shape-memory polymers is as active medical devices. Langer and Lendlein and coworkers[1,4] used shape memory polyurethane, which is both compatible with the body and biodegradable to produce coronary stents. Such stents could be compressed and fed through a tiny hole in the body into a blocked artery. Then, the warmth of the body would trigger the polymer's expansion into its original shape. Instead of requiring a second surgery to remove the material, the polymer would gradually dissolve in the body. Another successful example is a shape-memory degradable polyurethane suture developed by MnemoScience.[32] This suture can tie itself into a perfect knot in the body after being applied to wounds. It can be used to seal difficult wounds where access is limited.

From the previous studies, it can be seen that although the smart polyurethanes in the form of solution, emulsion, film, foam, bulk, and fiber have been being studied extensively, the report on the smart polyurethane hollow fiber is absent. In this work, we developed a smart hollow fiber via melt polymerization and melt spinning. The fiber's thermal, mechanical, and shape memory effect were investigated explicitly. As smart polyurethane hollow fiber has many special properties in comparison with cylindrical fiber, it may find many special applications. First, changes of the hollow fiber internal diameter will affect the physical properties of the products. If this kind of fiber is used in fabrics, the thermal sensitive heat transfer of the fabric will change according to the environment and body temperature. Second, the hollow fiber is proposed for use in the stuffing of pillows and mattresses, which can adjust to body contours for a comfortable feeling. If unloaded, after some time, they recover their original shapes. Furthermore, these kinds of hollow fibers with thermal sensitive internal diameter may be used in smart filtration, drug-controlled release, and liquid transportation *in vivo*.[33]

MATERIALS AND METHODS

Materials

The polyurethane was synthesized by using polycaprolactone diol (PCL)-4000 (International Laboratory, USA) as soft segment, 4,4-diphenylmethane diisocyanate (MDI; Aldrich Chemical), and ethylene glycol (EG; Sigma-Aldrich) as hard segment via melt polymerization. All glass vessels were cleaned and heated in a muffle to remove all moisture and organic residua before use. All chemicals were demoistured prior to use. The polyurethane was prepared by the pre-polymerization technique.[34,35] Pre-polymers were prepared by terminating PCL with excessive MDI on both ends at 80°C for half an hour. EG was added during the last stage. The reaction was controlled at below 90°C for 5 min. Then the polyurethane was further cured at 110°C for 4 h. The Fourier transform infrared spectra (FTIR) curve (obtained by using a Perkin-Elmer spectrometer 2000 FTIR) of the prepared polyurethane was shown in Figure 1. The —NCO group of MDI has four characteristic IR peaks: 2260–2280 cm^{-1} because of asymmetry stretching vibration; 1375–1395 cm^{-1} because of symmetry stretching vibration; 600–650 cm^{-1} because of out-of-plane bending vibration; and 590–600 cm^{-1} because of in-plane bending vibration.[36]

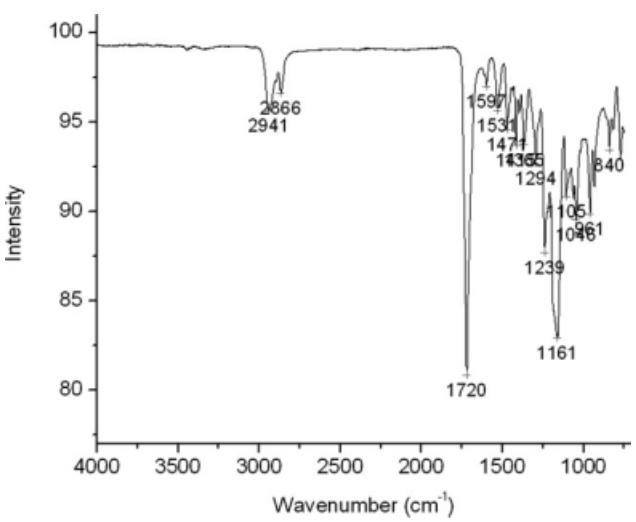

Figure 1 FTIR profile of the prepared polyurethane.

The peak at 2260–2280 cm^{-1} is prominent, which is frequently used to determine the existence of NCO. From Figure 1, it can be seen that the peak at 2260–2280 cm^{-1} completely disappears. This indicates that the reaction has finished. In this work, to make polyurethane with linear macromolecules, the mole ratio $[NCO]_{MDI}/([OH]_{EG} + [OH]_{PCL})$ was 1 : 1. Highly pure nitrogen was purged in the reactor to prevent the influence of atmospheric moisture. The polyurethane pellets were prepared by using a single extruder. Then the pellets were further cured in a vacuum oven (Shel Lab, USA) for 1 day.

Molecular weight testing

The number-average molecular weight (M_n) and weight-average molecular weight (M_w) of the polyurethane were determined with a multiangle laser light scattering apparatus (DAWN-DSP, Wyatt Technology, Santa Barbara, CA) combined with a P100 pump (Thermo Separation Products). The apparatus was equipped with a TSKGEL G5000 HHR column (7.8–300 mm) and an Optilab® rEX Refractive index detector. The refractive index increment (dn/dc) of polyurethane in dimethylformamide (DMF) was measured with a double-beam differential refractometer (DRM-1020, Otsuka Electronics, Japan) at 633 nm and 25°C to be 0.146 mL/g. The solvent used was high-performance liquid chromatograph grade DMF (Ajax Finechem) at 25°C. Astra software was used for data analysis.

Melt flow index

The melt flow index (MFI) was tested with a Davenport melt flow indexer MFI-10 (Fareham, UK). The samples were preheated in a barrel held at set temperature for 6 min. The amount of the polymer fed into the extruder was about 2.16 kg. The test was conducted five times at every experiment temperature.

Spinning

Before spinning, the polyurethane was dried in an oven to reduce moisture content to less than 100 ppm tested using a Micro-water Analyzer CHY-8 (Donghua University, China). The smart hollow monofilament was spun by using a self-fabricated laboratory spinning machine with highly pure nitrogen protection. The melt spinning temperature was 210°C. The cross-sectional shapes of the nozzle hole in the spinneret are shown in Figure 2. The quench temperature was room temperature. The winding speed was 100 m/min with an overfeed speed of 5 m/min. The smart hollow fiber is named thermal sensitive hollow fiber (THSF).

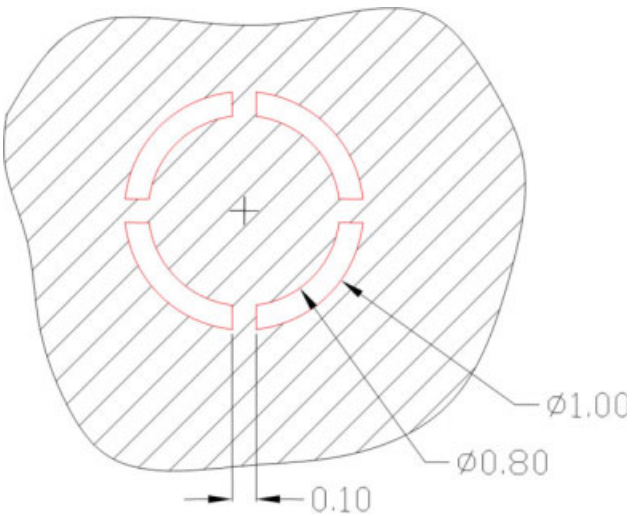

Figure 2 Cross-sectional shapes of the nozzle hole in the spinneret. [Color figure can be viewed in the online issue, which is available at www.interscience.wiley.com.]

Mechanical property

The mechanical properties were measured with Instron 4411 (Instron Corp., USA) according to the ASTM D 2256 standard. The sample gauge length between clamps was 20 mm and the stretching speed was 300 mm/min. Tests were conducted at room temperature (22°C) five times.

Thermal property investigation

The thermal properties of the smart hollow fiber were investigated by using a differential scanning calorimeter (DSC; Perkin-Elmer Diamond) in a nitrogen environment. Indium and zinc were used for calibration. Spinning oil on the filaments was removed before testing. The hollow fibers were first heated to 230°C at a heating speed of 10°C and kept for 1 min to get rid of thermal history. After that, it was cooled to −100°C at a cooling rate of 10°C/min and then heated to 240°C at a rate of 10°C/min. The thermograms were recorded for analysis.

X-ray diffraction analyses

The X-ray diffraction (XRD) data were recorded by using a Philips Analytical X-ray system (Philips Xpert XRD) at a voltage of 40 V and a current of 30 mA with a radiation wavelength of 1.542 Å. Spectra were obtained in a range of Bragg angles $2\theta = 10°–50°$ with a scanning step size of 0.02° and a time per step of 1 s.

Dynamic mechanical analyses

The dynamic mechanical analyses (DMA) test was carried out on a Perkin-Elmer Diamond dynamic mechanical analyzer operated in a tensile mode. The

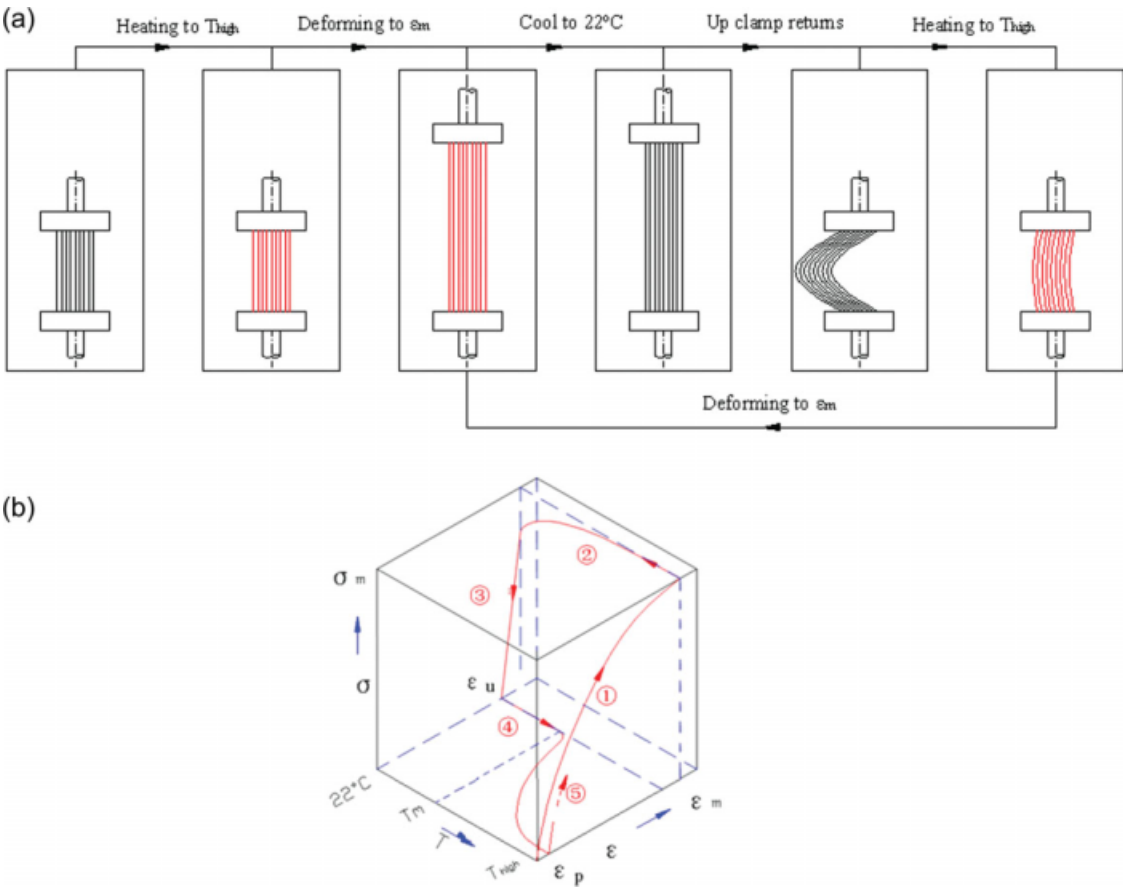

Figure 3 (a) Thermomechanical testing processes; (b) schematic thermomechanical cyclic tensile testing path. [Color figure can be viewed in the online issue, which is available at www.interscience.wiley.com.]

heating rate was 2°C/min; the frequency 1 Hz, and the oscillation amplitude 5.0 μm. The test was conducted over the temperature range from −120 to 200°C. The gauge length between the clamps was 15 mm. Usually, the modulus was calculated by the determined force, the cross-section area, and the caused strain employed in testing specimens. If the cross-section area was used in the calculation of stress and modulus, then the units will be GPa or MPa. However, for the fiber, the cross-section area that was not strictly regular was difficult to measure. In this test, the resulting data about the storage modulus were obtained by using linear density instead of cross-section areas similar to the calculation of fiber initial modulus in ASTM D 2256. The unit of the storage modulus was N/dtex.

Thermomechanical cyclic tensile testing

To quantify the smart fiber shape fixity ratio and recovery ratio, the thermo-mechanical cyclic tensile testing was conducted by using tensile tester (Instron 4466) equipment with a self-fabricated temperature controlled chamber. The sample gauge length was 20 mm. The cyclic tensile testing path is shown in Figure 3. ε_m is the defined as the maximum deformation in the cyclic tensile testing. It is 300% strain and 600% strain for this study. ε_u is the strain after unloading at T_{low}, and $\varepsilon_p(N)$ is the residual strain after recovering in the Nth cycle. The thermomechanical cycles for measuring the shape memory properties are as follows: (1) The fiber was first stretched to 100% elongation ratio at 65°C (T_{high}), which is above the switch transition temperature at a drawing speed of 10 mm/min.[37,38] (2) Subsequently, cool air was vented passively into the chamber to cool down the sample to 22°C and the temperature was kept for 15 min to fix the temporary elongation. (3) Then the upper clamp was returned to the original position at a speed of 40 mm/min and the fiber shrank from ε_m to ε_u because of instant elastic recovery. (4) Finally, the fiber was heated to 65°C to allow the shape memory recovery with resultant fiber elongation to return to ε_p. (5) After the cycle was completed, a second cycle began. The above procedure was carried out until five cycles had been completed. The fixity ratio (R_f) and recovery ratio (R_r) at the Nth cycle and total recovery ratio ($R_{r,tot}$) after the Nth cycle are calculated according to following equations[39,40]:

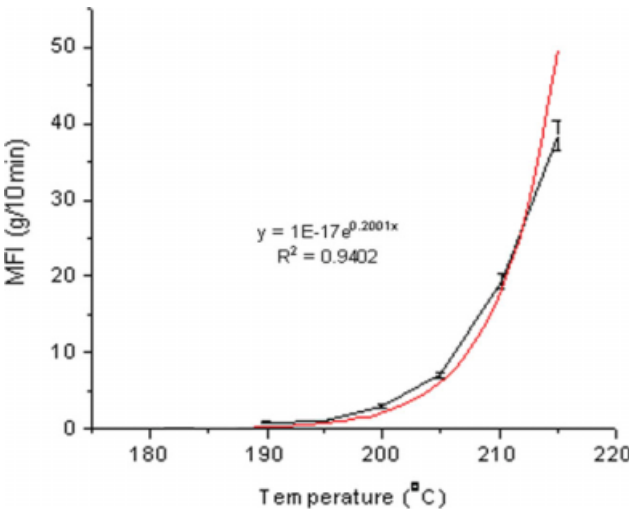

Figure 4 MFI of the prepared smart polyurethane with increasing temperature. [Color figure can be viewed in the online issue, which is available at www.interscience.wiley.com.]

$$R_f(N) = \varepsilon_u(N)/\varepsilon_m \times 100\%$$

$$R_{r.\mathrm{tot}} = \left[\varepsilon_m - \varepsilon_p(N)\right]/\varepsilon_m \times 100\%$$

$$R_r(N) = \left[\varepsilon_m - \varepsilon_p(N)\right]/\left[\varepsilon_m - \varepsilon_p(N-1)\right] \times 100$$

Thermal sensitive internal diameter

The hollow fiber cross-sections were taken by using an optical microscope (U-TEX/Electromicroscope Model UT901) equipped with scale. One lattice corresponded to 0.1 mm. Two kinds of stress were employed to deform the hollow fiber internal diameter: by stretching the hollow fiber in the fiber direction and by pressing the hollow fiber in the fiber transverse direction using forceps under an eye gauge. During the stretch method, first, the hollow fiber original cross-section image was taken by using an optical microscope; second, the hollow fiber was stretched to 200% elongation ratio in 65°C water to change internal diameter; third, the fiber was cooled in water at room temperature to fix the temporary internal diameter and a deformed cross-section image was taken. Finally, the deformed fiber was put into hot water at 65°C again so that the fiber's internal diameter recovered and a recovered cross-section image was taken. During the press method, first, the hollow fiber original cross-section images were taken by using an optical microscope; second, the hollow fiber was pressed flat in 65°C water to change internal diameter using forceps; third, the fiber was cooled in water at room temperature to fix the temporary cross-section and a deformed cross-section image was taken. After that, the deformed fiber was put into hot water at 65°C again so that the fiber internal cross-section recovered and then an image of the recovery cross-section was taken.

RESULTS AND DISCUSSION

MFI

The obtained polyurethane has an M_n of 1.42×10^5, an M_w of 2.57×10^5, and the polydispersity index of 1.80. The MFI of the polyurethane with an increasing temperature is shown in Figure 4. The Melt flow behavior of the synthesized polyurethane is similar to that of a thermoplastic polymer. The MFI is found to rise exponentially with increasing temperature. From Figure 4, it can be preliminarily determined that the appropriate temperature of melt spinning is at about 210°C. The prepared hollow fiber cross-section image taken by using an optical microscope (U-TEX/Electromicroscope Model UT901) is shown in Figure 5.

Mechanical property

The stress–strain curves of the TSHF derived from five experiments are shown in Figure 6. The TSHF has a tenacity of about 1.14 cN/dtex and breaking elongation of 682%. The tenacity is acceptable for textile applications in most circumstances.[41] In comparison with most other manmade fibers such as polyester and nylon, the mechanical strength of TSHF is lower. Polyester and nylon usually have high tenacity above 3.0 cN/dtex and low breaking elongation ratios. Polyester and nylon high tenacity is attributed to their higher overall orientation, strong intermolecular bonding in polyamide, and the high crystallinity of the molecular chain in polyester.[42] However, for the TSHF that shows high

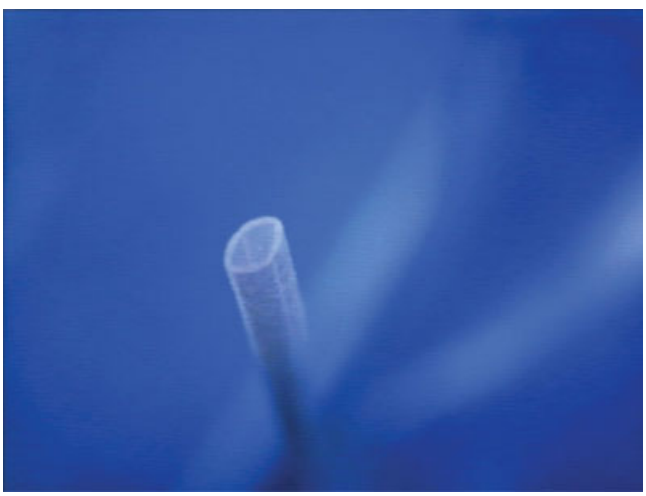

Figure 5 Cross-sectional image of the prepared hollow fiber. [Color figure can be viewed in the online issue, which is available at www.interscience.wiley.com.]

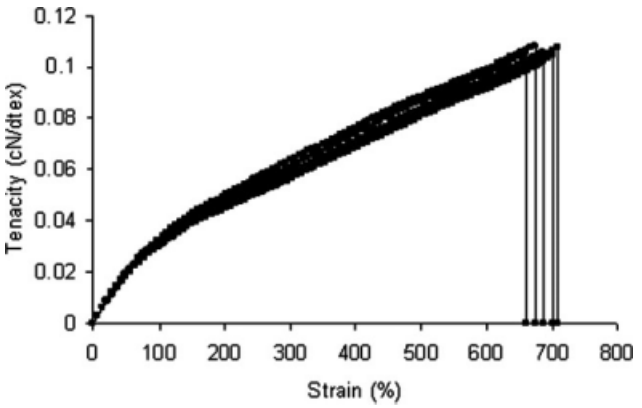

Figure 6 Static stress–strain curves of the TSHF.

shape fixity ratios and shape recovery ratios, the elongation at break is much higher compared with those of polyester and nylon.

In the TSHF, the high molecular weight PCL provides the fiber with high breaking elongation ratios and the hydrogen bonded hard segment supplies it with a high mechanical strength.[43,44] The TSHF mechanical strength can be improved through increasing hard segment content or molecular orientation. However, these two methods are at the expense of TSHF stretchablility and melt processability.

Differential scanning calorimeter analyses

The DSC curves of the pure PCL and TSHF in the cooling and heating scan are shown in Figure 7. The detailed melting temperature, crystallizing temperature, corresponding enthalpy, and crystallinity are tabulated in Table I. The thermograms of both pure PCL and TSHF show the exothermic crystallization peak in the cooling scan and the endothermic melting peak in the heating scan. The melting transition temperature of TSHF is at about 41.2°C. This thermal transition is attributed to the PCL soft-segment phase transition in the TSHF. The crystallinity of TSHF is much lower in comparison with that of pure PCL. This is because, in the polyurethane system, the hard segment intrudes into the well-formed PCL phase and interferes with the PCL crystalline behavior. No obvious hard segment phase endothermic peak appears in the TSHF heating scanning. This may be due to the fact that the hard segment content in the TSHF is relatively low, and consequently, no well-ordered hard segment phase forms. According to previous studies, no crystallized structure of hard segment will form unless the hard segment content is very high such as above 50 wt %.[25,47] As at an ambient temperature, the soft-segment phase is partially crystallized, and the TSHF is not completely elastic as those in elastic polyurethane fibers.[48,49]

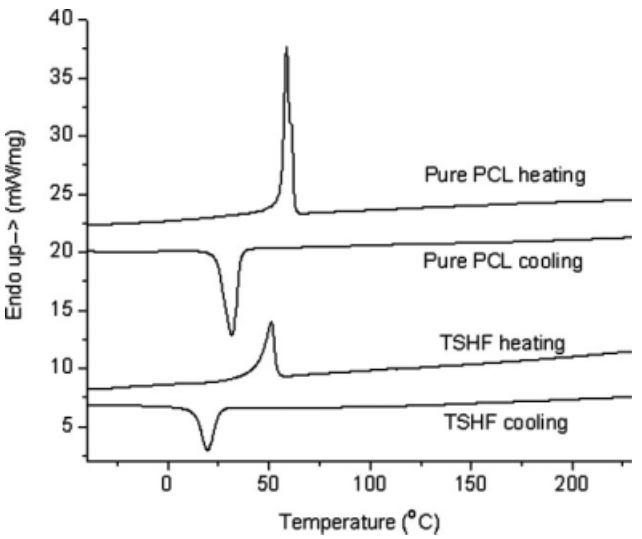

Figure 7 The DSC curves of the pure PCL and the TSHF.

TABLE I
Thermal Transition Temperature and Crystallinity of Pure PCL and TSHF

		T_c/T_m (°C)	ΔH (J/g)	Crystallinity (%)
PCL-4000	Cooling	31.6	53.0	37.9
	Heating	58.6	53.2	38.0
TSHF	Cooling	19.6	28.4	20.3
	Heating	41.2	27.9	19.9

T_m is crystal melting temperature; ΔH is the heat of fusion. The soft-segment crystallinity was calculated from the enthalpy data ΔH of the crystallization by using the 140 J/g enthalpy value for fusion of 100% crystalline PCL given by Crescenzi et al.[45,46]

XRD analysis

To further investigate the crystalline properties, the crystalline structures and unit cell parameters of the pure PCL and TSHF were studied by using XRD. The XRD patterns are shown in Figure 8. The peaks of XRD curves were separated and areas of the X-ray scattering of every amorphous phase broad peak and sharp crystalline phase peak were integrated by using the Philips Xpert XRD system software. The degree of crystallinity was calculated by using the method described by Young and Lovell.[50] The percentage crystallinity (X_c) within the sample was calculated using the equation:

$$X_c = \left(\frac{\sum_i A_{ci}}{\sum_i A_{ci} + \sum_j A_{Aj}} \right) \times 100\%$$

where A_c is the area of the X-ray diffraction curve due to scattering from the crystalline phase, and A_a

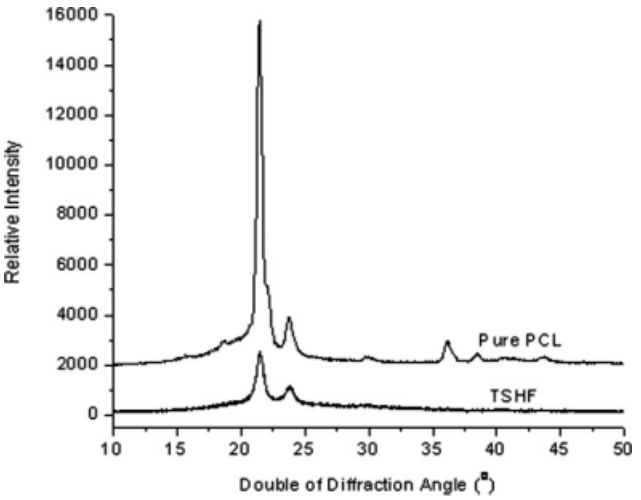

Figure 8 XRD patterns of pure PCL and the TSHF.

is the area of the X-ray diffraction curve due to scattering from amorphous.

The peaks separating results and calculated crystallinities are presented in Table II. The thermal property results are generally consistent with those obtained from DSC analysis. The soft-segment phase in the TSHF has high crystallinity even though the PCL crystallization in the TSHF is suppressed by the employed hard segment.[51]

The average crystallite size was determined coarsely by using the Debye-Scherrer formula[52,53]: $L_{(hkl)} = k\beta/\beta\cos\theta$. Here β is the applied X-ray wavelength $\beta_{Cu} = 1.542$ Å; θ is diffraction angle; $k = 0.89$; β is full-width at half maximum (FWHM) in radians. Marchessault[54] found the unit cell of PCL was orthorhombic with dimensions $a = 7.496$ Å, $b = 4.974$ Å, and $c = 17.297$ Å. From Figure 8 we can see that both the pure PCL and the TSHF have two prominent diffraction peaks. The peaks of TSHF at 21.48° can be attributed to the (110) plane diffraction of PCL. The peak at 23.79° is because of the (200) plane diffraction.[54] The unit cell parameters of TSHF with those of pure PCL as references are presented in Table III. For (110) plane, the average crystallite size is lower compared with that in pure PCL. For (220) plane, the average crystallite is also smaller in comparison to pure PCL.

TABLE II
The Results of Peak Separation and Calculated Crystallinity

Sample		Peak position 2θ (°)	FWHM (°)	Height (count)	Area (count)	Crystallinity
PCL-4000	1	20.61	7.07	732.7	6298.1	
	2	21.43	0.44	9280.8	5001.1	
	3	22.11	0.37	1171.2	552.7	
	4	23.78	0.55	959.9	640.1	
	5	29.92	1.27	126.1	194.3	
	6	36.15	0.53	591.9	383.0	
	7	38.45	0.39	198.5	94.8	
	8	41.10	17.04	162.6	3367.8	41.53%
As-spun SMF	1	21.09	7.19	106.6	649.13	
	2	21.48	0.7	671.76	519.71	
	3	23.79	0.82	213.69	206.82	
	4	25.75	0.58	97.6	1977.08	
	5	40.5	1.07	14.84	13.8	21.99%

TABLE III
The Lattice Parameters of the TSHF

	(110)			(200)		
Sample	2θ	FWHM (°)	L (hkl)	2θ	FWHM (°)	L (hkl)
PCL	21.43	0.44	181.64	23.78	0.55	145.91
TSHF	21.48	0.70	114.19	23.79	0.82	97.87

Dynamic mechanical analyses

The elastic modulus (E') and loss tangent (tan δ) of the TSHF over the temperature range from −120 to 200°C are presented in Figure 9. It can be seen that from −55 to 50°C, the E' has two sharp decreases. The first decrease, emerging in the vicinity of −55°C, can be ascribed to the glass transition of the soft segment as can be seen from the tan δ temperature curve. The second decrease is owing to the melting transition of soft segment at about 41°C, which is more obvious in the fiber DSC curve. The slight differences of the thermal transition temperature between DSC and DMA are due to the different thermal histories. At temperatures above about 41°C when the soft-segment crystals melt, the mechanical strength of the TSHF is mostly contributed by the hard segment,[47] as can be seen from the plateau region of E'. Upon heating above 160°C, another decrease in E' is observed, indicating that the

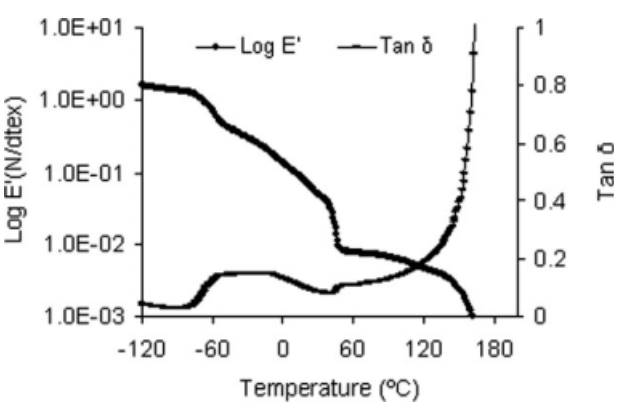

Figure 9 Log E′–temperature curve and tan δ–temperature curve of the TSHF.

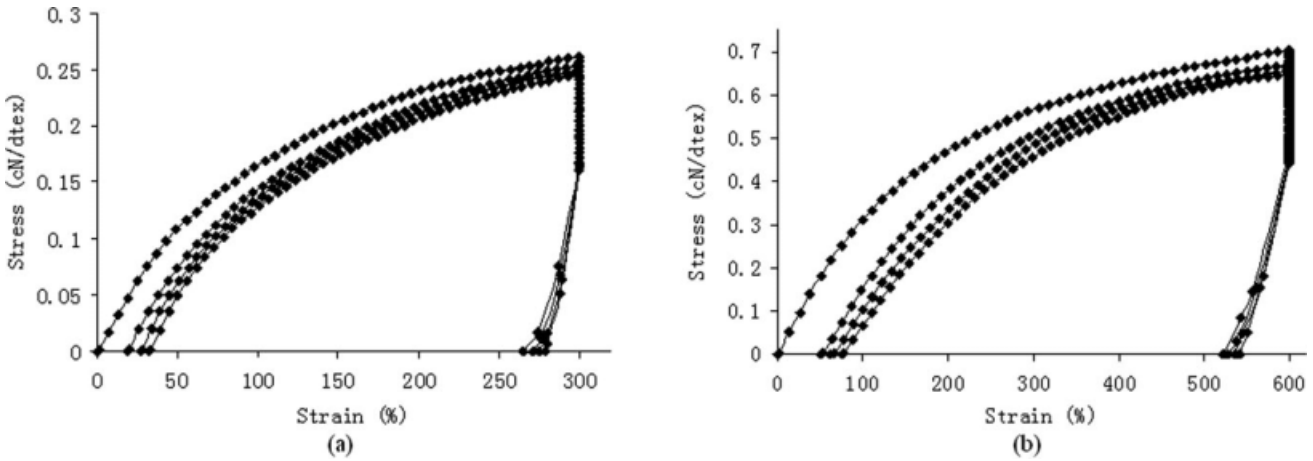

Figure 10 The cyclic tensile testing result of the TSHF: (a) set maximum elongation 300%; (b) set maximum elongation 600%.

physical cross-linking between hard segment begins to be destroyed.

Thermomechanical cyclic tensile testing

The cyclic strain–stress curves of TSHF obtained by thermo-mechanical cyclic tensile testing by 300% elongation mode and 600% elongation mode are shown in Figure 10. The significant difference between the first thermal cycle and the remaining cycles is because of reorganization of polyurethane molecules involving molecule orientation, crystallization, and weak point broken during elongation. After the first cycle, the thermo-mechanical properties become very similar. The detailed shape fixity ratios and recovery ratios are tabulated in Table IV. The TSHF has the fixity ratios of more than 80% and recovery ratios of more than 90% at 300% maximum elongation mode. The fixity ratio is above 85.0% and recovery ratio above 90% at 600% maximum elongation mode. At 65°C in the first cycle, the stress is 0.26 cN/dtex at 300% elongation ratio and 0.70 cN/dtex at 600% elongation ratio.

Thermally tunable internal diameter

The change of hollow fiber internal diameter will influence the physical properties of its products. Therefore, in this work, the thermally tunable cross-section of the hollow fiber was investigated. The images of the original cross-section, deformed cross-section, and recovery cross-section of the TSHF are shown in Figures 11 and 12. In Figure 11, the deformation is conducted by longitude stretching. In Figure 12, the deformation is carried out by pressing the fiber in the transverse direction. From Figure 11, it can be seen that the hollow fiber internal diameter has become smaller after stretching, and the shape is fixed at room temperature. After being put in hot water at 65°C, the fiber cross-section recovers its original shape. The same result is obtained in Figure 12 where deformation is conducted by pressing the fiber in a transverse direction. The deformed flat shape is fixed, and after being heated to 65°C, it recovers to its original shape.

The thermo-mechanical cyclic tensile properties and the thermally adjustable internal hole diameter of the TSHF can be illustrated as follows. In the deformed state, the soft-segment phase in the TSHF has a high crystallinity as has been proven by DSC. The hard segment forms a hard segment phase through strong hydrogen bonding, which has been tested by DMA results. When the TSHF is heated from room temperature to 65°C, which is above the soft-phase melting transition temperature (T_{trans}), the PCL phase melts. When it is stretched, the fiber can be easily extended. If the temperature is cooled to below T_{trans}, the soft segment crystallizes and, as a result, the internal stress is stored in the material

TABLE IV
Shape Fixity and Recovery Ratios of TSHF

Circle no.	$\varepsilon_p(N)$	$\varepsilon_u(N)$	$[R_f(N)]$	Stress at maximum strain (cN/dtex)	$R_{r,tot}$ (N)	R_r (N)
Set maximum elongation 300%						
1	0.0%	250.0%	83.3%	0.26	100.0%	
2	19.3%	256.0%	85.3%	0.25	93.6%	93.6%
3	27.0%	262.0%	87.3%	0.25	91.0%	97.2%
4	32.3%	264.0%	88.0%	0.25	89.3%	98.1%
Set maximum elongation 600%						
1	0.0%	522.0%	87.0%	0.70	100.0%	
2	51.0%	529.0%	88.2%	0.67	91.5%	91.5%
3	64.0%	536.0%	89.3%	0.66	89.3%	97.6%
4	75.0%	542.0%	90.3%	0.65	87.5%	97.9%

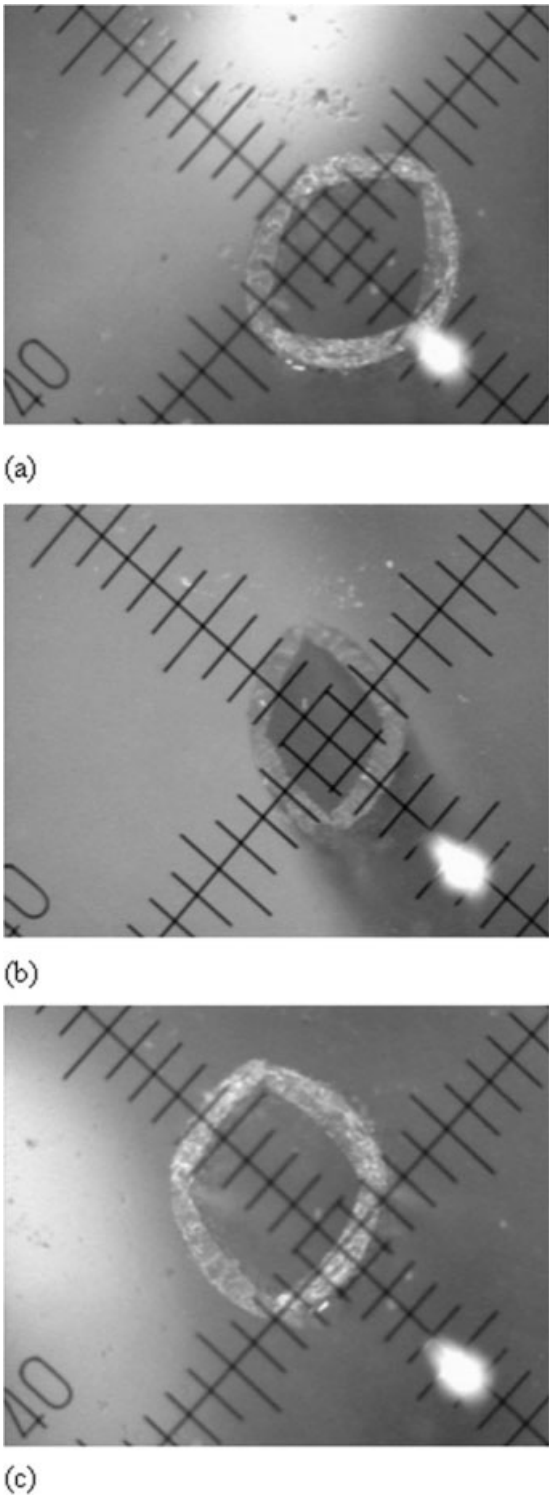

Figure 11 Thermally adjustable internal holes of the TSHF (deformed by longitude stretching) (a, original shape; b, deformed shape, c, recovered shape).

and associated deformation is fixed temporally. However, if it is reheated to above T_{trans}, the soft-segment phase becomes flexible and the fiber resumes to the original length as a result of releasing internal stress stored among hard segment.

CONCLUSION

In this work, a thermoplastic shape memory polyurethane was synthesized via melt polymerization, and a corresponding shape memory hollow fiber was fabricated via melt spinning. The fiber

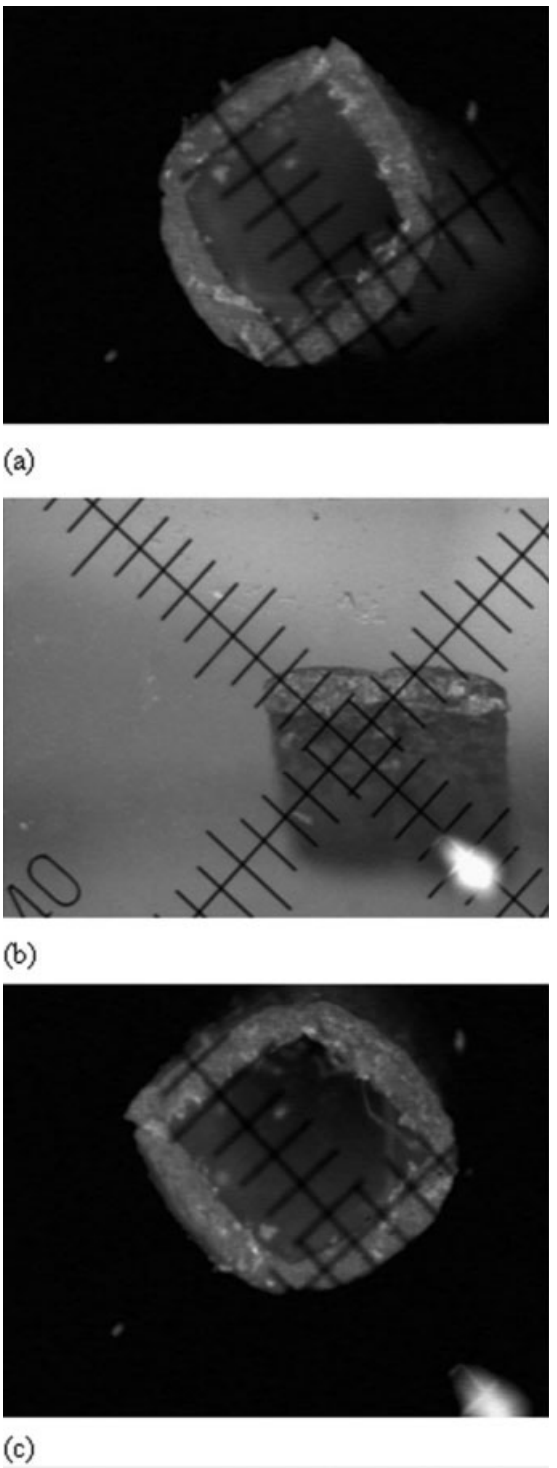

Figure 12 Thermally adjustable internal holes of the TSHF (deformed by transverse pressing) (a, original shape; b, deformed shape, c, recovered shape).

mechanical properties, especially shape memory effect, were characterized by static tensile, thermomechanical cyclic tensile testing. The results from DSC, XRD, and DMA were used to illustrate the mechanism governing the mechanical properties and shape memory effect especially. The shape memory hollow fiber main properties were as follows.

1. The hollow fiber switching temperature was the melting transition temperature of the soft-segment phase at about 41°C.
2. The hollow fiber had a tenacity of about 1.14 cN/dtex, and strain at break of 682%. The shape fixity ratio was above 80% and the recovery ratio above 90%.
3. The internal diameter of the hollow fiber could be noticeably changed and the deformed fiber cross-section could be well fixed; after being heated above the soft-segment phase melting transition temperature, the hollow fiber internal hole recovered to its original diameter.
4. The changes of the hollow fiber internal diameter affect the physical properties of the product. This fiber may be used in smart textiles for thermal management, or as stuffing of pillows and mattresses, which can adjust to body contours. Furthermore, this kind of hollow fibers with thermal sensitive internal diameter may be used in smart filtration, drug-controlled release, and liquid transportation *in vivo*.

References

1. Lendlein, A.; Langer, R. Science 2002, 96, 1673.
2. Kelch, S.; Steuer, S.; Schmidt, A. M.; Lendlein, A. Biomacromolecules 2007, 8, 1018.
3. Alteheld, A.; Feng, Y.; Kelch, S.; Lendlein, A. Angew Chem Int Ed 2005, 44, 1188.
4. Lendlein, A.; Schmidt, A. M.; Langer, R. Presented at the Proceedings of the National Academy of Sciences, USA, 2001.
5. Hayashi, S.; Tasaka, Y.; Hayashi, N.; Akita, Y. Development of Smart Polymer Materials and Its Various Applications (Technical Review); Mitsubishi Heavy Industries: 2004; Vol. 41, p 1.
6. Tobushi, H.; Hayashi, S.; Hoshio, K.; Miwa, N. Smart Mater Struct 2006, 15, 1033.
7. Hayashi, S.; Tasaka, Y.; Hayashi, N.; Akita, Y. Development of Smart Polymer Materials and Its Various Applications (Technical Review); Mitsubishi Heavy Industries: 2004; Vol. 41, p 3.
8. Mondal, S.; Hu, J. L. Carbohydr Polym 2007, 67, 282.
9. Meng, Q. H.; Hu, J. L. Polym Adv Technol 2008, 19, 131.
10. Meng, Q. H.; Hu, J. L.; Zhu, Y.; Lu, J.; Liu, Y. Smart Mater Struct 2007, 16, 1192.
11. Jung, Y. C.; So, H. H.; Cho, J. W. J Macromol Sci B: Phys 2006, 45, 453.
12. Yang, B.; Huang, W. M.; Li, C.; Li, L. Polymer 2006, 47, 1348.
13. Langer, R. S.; Andreas, L. U.S. Pat. 6,388,043-B1 (2002).
14. Crowson, A. In Smart Materials Based on Polymeric Systems, Smart Structures and Materials; Smart Materials Technologies and Biomimetics: San Diego, California, 1996.
15. Tobushi, H.; Hara, H.; Yamada, E.; Hayashi, S. Proceedings of the 3rd International Conference on Intelligent Materials; Lyon, France, 1996; p 418.
16. Tobushi, H.; Hashimoto, T.; Ito, N.; Hayashi, S.; Yamada, E. J Intell Mater Syst Struct 1998, 9, 127.
17. Hu, J. L. Shape Memory Polymers and Textiles; Woodhead Publishing Limited: Cambridge, England, 2007.
18. Draper, D. World Spots Activewear 2001, 7, 22.
19. Hu, J. L.; Ding, X. M.; Tao, X. M. J China Text Univ 2002, 19, 89.
20. Fan, H. J.; Hu, J. L.; Ji, F. L. Presented at the World Textile Conference 4th AUTEX Conference, Roubaix, France, 22–24 June, 2004.
21. Mattila, H. R. Intelligent Textiles and Clothing; Woodhead Publishing Limited: Cambridge, England, 2006.
22. Mondal, S.; Hu, J. L. Res J Text Apparel 2002, 6, 75.
23. Li, Y.; Chung, S.; Chan, L.; Hu, J. L. Text Asia 2004, 35, 32.
24. Shishoo, R. Int J Clothing Sci Technol 2002, 14, 201.
25. Zhu, Y.; Hu, J. L.; Yeung, L. Y.; Lu, J.; Meng, Q. H.; Chen, S. J.; Yeung, K. W. Smart Mater Struct 2007, 16, 969.
26. Zhu, Y.; Hu, J. L.; Yeung, L. Y.; Liu, Y.; Ji, F. L.; Yeung, K. W. Smart Mater Structures 2006, 15, 1385.
27. Ji, F. L.; Zhu, Y.; Hu, J. L.; Liu, Y.; Yeung, L. Y.; Ye, G. D. Smart Mater Struct 2006, 15, 1547.
28. Tobushi, H.; Matsui, R.; Hayashi, S.; Shimada, D. Smart Mater Struct 2004, 13, 881.
29. Lendlein, A.; Langer, R. S. U.S. Pat. WO/2004/073690, PCT/US2004/004776 (2004).
30. Marco, D.; Eckhouse, S. U.S. Pat. 20,070,156,248 (2006).
31. Huang, W. M.; Lee, C. W.; Teo, H. P. J Intell Mater Syst Struct 2006, 17, 753.
32. Mnemoscience, http://www.mnemoscience.de/ (accessed 12/27/07).
33. Ltd, U. Presented at the Light Weight Hollow Fibre Thermally Insulating Fabrics for Winter Clothings and Sportswear, Japan, 1996.
34. Zhang, Z. R. China Pat. CN20,020,150,720 (2004.
35. Cherubini, J. U.S. Pat. 5,415,623 (1995).
36. Merck, D. Merck FT-IR Atlas; VCH Publishers: New York, 1988.
37. Zhu, Y.; Hu, J. L.; Yeung, K. W; Fan, H. J.; Liu, Y. Q. Chin J Polym Sci 2006, 24, 173.
38. Kim, B. K.; Lee, S. Y.; Xu, M. Polymer 1996, 37, 5781.
39. Meng, Q. H.; Hu, J. L.; Zhu, Y.; Lu, J.; Liu, Y. J Appl Polym Sci 2007, 106, 2515.
40. Meng, Q. H.; Hu, J. L.; Zhu, Y. J Appl Polym Sci 2007, 106, 837.
41. Mark, H. F.; Atlas, S. M.; Cernia, E. Man-Made Fibers Science and Technology; Wiley: 1968; Vol. 3.
42. Yao, M.; Zhou, J.; Huang, S.; Shao, L.; An, R.; Fan, D. Textile Materials, 2nd ed; Textile Industry Publishing House: Peking, 1990.
43. Bhat, G.; Chand, S.; Yakopson, S. Thermochim Acta 2001, 367/368, 161.
44. Fourne, F. Synthetic Fibers Machines and Equipment, Manufacture, Properties; Hanser: Munich, 1999.
45. Crescenzi, V.; Manzini, G.; Calzolari, G.; Borri, C. Eur Polym J 1972, 8, 449.
46. Luo, N.; Wang, D.; Ying, S. Polymer 1996, 37, 3577.
47. Korley, L. T. J.; Pate, B. D.; Thomas, E. L.; Hammond, P. T. Polymer 2006, 47, 3073.
48. Lee, H. S.; Ko, J. H.; Song, K. S.; Choi, K. H. J Polym Sci Part B: Polym Phys 1997, 35, 1821.
49. Fabricius, M.; Gries, T.; Wulfhorst, B. Chem Fibers Int 1995, 45, 1995.
50. Young, R. J.; Lovell, P. A. Introduction to Polymers, 2nd ed.; Chapman and Hall: London, 1991.
51. Lin, J. R.; Chen, L. W. J Appl Polym Sci 1998, 69, 1563.
52. Patterson, A. L. Phys Rev 1939, 56, 978.
53. Mo, L. K. Z. S.; Moon, Y. B.; Kobayashi, M.; Heeger, A. J.; Wudl, F. Macromolecules 1985, 18, 1972.
54. Marchessault, H. B. A. R. H. Acta Crystallogr B 1970, 26, 1923.